# Oxygen-Evolving Mn Cluster in Photosystem II: The Protonation Pattern and Oxidation State in the High-Resolution Crystal Structure

Artur Galstyan, Arturo Robertazzi, and Ernst Walter Knapp*

Department of Biology, Chemistry and Pharmacy, Institute of Chemistry and Biochemistry, Freie Universität Berlin, Fabeckstrasse 36a, D-14195 Berlin, Germany

S *Supporting Information*

ABSTRACT: Extensive quantum chemical DFT calculations were performed on the high-resolution (1.9 Å) crystal structure of photosystem II in order to determine the protonation pattern and the oxidation states of the oxygen-evolving Mn cluster. First, our data suggest that the experimental structure is not in the S_1-state. Second, a rather complete set of possible protonation patterns is studied, resulting in very few alternative protonation patterns whose relevance is discussed. Finally, we show that the experimental structure is a mixture of states containing highly reduced forms, with the largest contribution (almost 60%) from the S_{-3}-state, $Mn(II,II,III,III)$.[1]
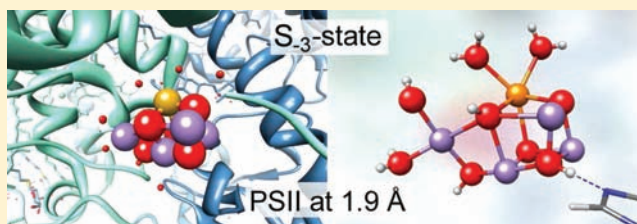
INTRODUCTION

Photosystem II (PSII) is one of the fundamental protein complexes that govern life on earth.[2] It catalyzes the decomposition of water into protons, electrons and produces molecular oxygen as waste product. This light-driven endoenergetic reaction is performed by the oxygen-evolving complex (OEC), which contains a manganese cluster. Understanding the mechanism of the OEC in PSII is a tremendous challenge for the scientific community. It is central to develop artificial photosynthetic systems that can solve the existing energy problem producing oxygen and hydrogen from water with solar power.

In the past decade, several scientific groups solved the structure of PSII by X-ray crystallography improving the resolutions from 3.8 Å,[3] 3.7 Å,[4] 3.5 Å,[5] 3.0 Å[6] to 2.9 Å.[7] The crystal structures clarified that the Mn cluster of the OEC is a Mn_4Ca complex. However, important structural details, such as for instance the position of the μ−oxo bridges and water ligands, were lacking. In addition, the Mn cluster may have suffered radiation damage by X-ray photo-reduction,[8−10] due to the intensive synchrotron radiation during the measurements. We would like to remark that a number of theoretical studies based on the previous lower resolution structural data[5−7] were performed that focused on the structure and function of the Mn cluster.[11−15]

In 2011, however, the structure of PSII was solved with an unprecedented level of accuracy (1.9 Å resolution),[16] which revealed new details. In particular, the cubane-like Mn cluster (with the chemical composition of Mn_4CaO_5) is constituted of a Ca atom and three Mn atoms, connected by four oxygens (O1, O2, O3, O5) as well as an "external" Mn (Mn4) connected via O5 and a fifth oxygen atom (O4) (Figure 1). Importantly, in the high-resolution crystal structure, all ligands

of the Mn cluster were determined, four of which were identified as water molecules.[16] With these important structural details, a new round has been opened in the effort to understand the function of the Mn cluster in PSII.

To reduce X-ray damage, a slide−oscillation technique was employed[16] that should ensure the Mn cluster to remain in the dark-stable S_1-state $[Mn(III,III,IV,IV)]$. However, a possible X-ray photo-reduction of the Mn cluster may have occurred, and has become a matter of debate.[17,18] In fact, it is now believed that the Mn cluster is in a more reduced state. A recent computational study on the Mn_4CaO_5 cluster[17] put forward the hypothesis that the crystal structure[16] corresponds to a mixture of different oxidation states rather than simply to the S_1-state. Yet, the precise nature of the oxidation state of the catalytic center in the PSII crystal structure is still an open question.

Besides the uncertainty about the oxidation state of the Mn cluster, the PSII crystal structure cannot show the protonation pattern of the μ−oxo oxygens and Mn ligands. This information is, however, crucial to provide a detailed description of the catalytic mechanism of water oxidation at a molecular level. Very recently, two more theoretical studies based on the PSII high-resolution structure appeared.[19,20] These studies did not solve the uncertainty about the oxidation and protonation state of the Mn cluster in the PSII crystal.

Alternative structural information on the PSII Mn cluster can be obtained from EXAFS spectra.[18,21] They yield very precise information, but need complementary data, for instance, from a crystal structure, to build a complete three-dimensional molecular model for systems as complex as the Mn cluster in PSII. EXAFS spectral data are recorded at much lower X-ray
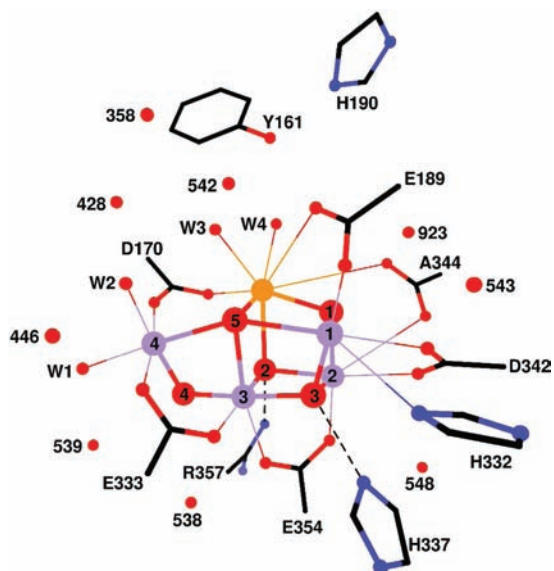
Figure 1. Complete OEC-model considered in the quantum chemical computations based on the PSII crystal structure.[16] The structure is shown schematically with Mn_4CaO_5-cluster, ligands and nearest neighbor residues. The atoms of the Mn_4CaO_5 cluster are highlighted by using large spheres. Ca and Mn metals are shown as orange and violet spheres, respectively. The five oxygens bridging Mn and Ca are shown as large red spheres. The numbers denoting the Mn and O atoms of Mn_4CaO_5 cluster are given inside the spheres. For the sake of clarity, water molecules are represented only by the oxygens (small red spheres) with corresponding residue numbers. We make use of the following notation: W1, W2, W3, and W4 for the water ligands HOH1000, HOH999, HOH541, and HOH540, respectively. Ligand atoms are connected with corresponding atoms of Mn_4CaO_5 by solid lines; hydrogen bonding partners are connected by dashed lines. The acidic group A344 is a C-terminal alanine.

intensity than protein crystal structures.[21] Therefore, those results are not subject to radiation damage. However, no EXAFS spectra of the Mn cluster in highly reduced states are available. Hence, these data cannot be used to identify such states.

In this work, the structural features of both oxidation and protonation states of the Mn cluster are addressed by performing extensive density functional theory (DFT) calculations on the most recent high-resolution PSII crystal structure[16] (Figure 1). Our data confirm that the excess of electrons generated by synchrotron radiation caused radiation damage, and in fact indicate that the PSII crystal structure contains a combination of different highly reduced OEC states.

■ RESULTS AND DISCUSSION

Oxidation States of Mn_4CaO_5 and Protonation States of W2 and His337. First, we would like to remark that the monomer A of the high-resolution PSII crystal structure[16] was employed in all calculations, since it is more complete. In the S_1-state, the total charge of the OEC-model (OEC-charge) as displayed in Figure 1 is +1, if we agree that all considered crystal waters are H_2O, all acidic groups deprotonated, all basic groups protonated, all histidines neutral, Tyr161 protonated (charge neutral), and all five μ−oxo oxygens deprotonated. The corresponding charge of the Mn-CORE (Mn_4CaO_5) alone, without the six acidic ligands and the basic R357, is +6.

On the basis of a careful analysis of the PSII crystal structure, several alternative protonation patterns of Mn_4CaO_5, W2 and

His337 were investigated (Figure 2) and are briefly discussed here. The short distance between the positively charged
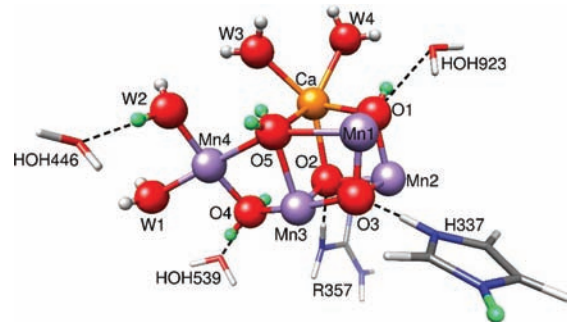

Figure 2. Protonation states in the OEC-model. Only relevant molecular groups are shown. Gray spheres show hydrogen atoms, which we consider to be present in S_1 and the more reduced states. Hydrogen bonding partners are connected by dashed lines. Green colored spheres show positions, which may be occupied by protons resulting in a total of $2^3 \times 3^2 = 72$ different protonation patterns. In a first stage, the protonation of W2 and His337 is fixed resulting in $2 \times 3^2 = 18$ possible protonation patterns.

hydrogen atoms of Arg357 and O2 should prevent the μ−oxo oxygen from carrying a hydrogen atom. In fact, O2 is very likely to act as hydrogen bond acceptor group (Figure 2). Oxygen O1 may either carry one or no hydrogen atoms, while the possibility that O1 may bind two hydrogen atoms is ruled out, since it is strongly bound to two Mn atoms (Mn−O1 distances of about 1.8 Å) and to one Ca atom (Ca−O1 distance 2.5 Å). Oxygen O4 is only bound to two Mn atoms (Figure 2). Albeit connected with three Mn and the Ca, oxygen O5 is only loosely bound to Mn1 and Mn3 with rather large distances of about 2.6 Å. Therefore, both oxygens O4 and O5 may bear none, one or even two protons. The protonation state of O3 depends on that of its H-bond partner His337. The distance of 2.6 Å between O3 and N_ε^{His337} indicates that O3 and His337 are strongly hydrogen-bonded[16] and should share one proton. Thus, for all five μ−oxo oxygens of the Mn cluster, all reasonably possible protonation pattern scenarios are considered.

According to monomer A of the PSII crystal structure,[16] the bond length of Mn4 to the W2 water oxygen is by 0.14 Å shorter than that to the W1 water (Mn4−O^{W1} distance 2.22 Å). This may be an indication that W2 is in the deprotonated form OH^-, although the differences are within the experimental uncertainty and make it difficult to discriminate between the OH^- and H_2O forms of the two waters. In contrast, in monomer B,[16] the bond lengths (Mn4−O^{W1} and Mn4−O^{W2}) have practically the same values (difference 0.03 Å). In fact, the average bond lengths of the two water oxygens (W1 and W2) to Mn4 are nearly the same for the monomers A and B, both about 2.15 Å. For W1 we can exclude the OH^- form, since it has two H-bond partners functioning as H-bond acceptors (−COO^- group of Asp61 and the backbone −C=O group of Ser169). However, for W2, both forms, OH^- and H_2O, may be possible and therefore are taken into account in our calculations. All other titratable residues considered here are kept in the standard protonation state, that is, acidic groups and histidines are deprotonated, except for His337; crystal waters are considered to be charge neutral except for W2; Tyr161 is protonated (charge neutral).

Table 1. Results of Quantum Chemical Computations (rmsd, Energy, OEC-Charge) in the S_1-State Are Given for the Stage 1, Considering 18 Different Protonation Patterns of the Mn-CORE with Variable Protonation for O1, O4, and O5 while the Protonation of W2 (OH^-) and His337$^+$ Is Fixed^a

charge group	no.	protonation state	rmsd$_{CORE}$ [Å]	relative energy [kcal/mol]	OEC-charge^b
I	1.	**O5−O4**	**0.276**	**0.00**	+1
II	2.	O5H−O4	0.227	24.39	+2
	3.	**O5−O4H**	**0.280**	**0.00**	
	4.	O5−O4−O1H	0.285	8.63	
III	5.	O5HH−O4	0.289	19.23	+3
	6.	**O5H−O4H**	**0.219**	**0.00**	
	7.	O5−O4HH	0.265	26.07	
	8.	O5H−O4−O1H	0.202	30.22	
	9.	O5−O4H−O1H	0.257	2.89	
IV	10.	O5HH−O4H	0.231	13.41	+4
	11.	O5H−O4HH	0.272	8.03	
	12.	O5HH−O4−O1H	0.267	41.24	
	13.	**O5H−O4H−O1H**	**0.212**	**0.00**	
	14.	O5−O4HH−O1H	0.274	13.60	
V	15.	O5HH−O4HH	−^{c}	−	+5
	16.	O5HH−O4H−O1H	0.242	5.38	
	17.	**O5H−O4HH−O1H**	**0.285**	**0.00**	
VI	18.	O5HH−O4HH−O1H	−^{c}	−	+6

^{a}For simplicity we left out the suffix −His337$^+$−W2$^-$ when characterizing the protonation. The rmsd values of the Mn-CORE are given relative to the coordinates of the PSII crystal structure.[16] Different states with the same number of protons are grouped together. Relative energies are comparable only within the same charge group. In each charge group, the OEC-model with lowest energy is rendered in bold. The corresponding absolute energies are given in Table S1 of Supporting Information. ^{b}Total charge of the OEC-model as depicted in Figure 1. ^{c}Deprotonates spontaneously during geometry optimization.

From this analysis, it is clear that the number of 72 possible protonation patterns (see Figure 2), which need to be considered in combination with six possible oxidation states (S_1−S_{-4}) is very large. To investigate the properties of all these states at the DFT level would be computationally too demanding (each of the models contains between 141 and 146 atoms). To achieve a trade-off between completeness, accuracy and efficiency, a three-stage procedure was employed.

Stage 1 (Protonation of Mn-CORE): since the Mn_4CaO_5 cluster (Mn-CORE) was claimed to be in the S_1-state,[16] we started with this assumption searching for the most likely protonation patterns of the central Mn_4CaO_5-cluster. In this stage (and the following stage 2), the protonation pattern of W2 and His337 was kept fixed to be OH^- and His$^+$, respectively, resulting in a total of 18 possible protonation states (see Figure 2). In stage 3, where we have considered the more reduced states, this restriction was relaxed.

Stage 2 (Oxidation of Mn-CORE): having determined the most likely protonation states of the Mn-CORE in stage 1, different oxidation states, including highly reduced states each with a range of possible protonation states, were explored in stage 2.

Stage 3 [Protonation of Mn-CORE-extended (Mn_4CaO_5− W2-His337)]: based on the most promising protonation patterns of the Mn-CORE determined in stage 1 and 2, the protonation of the ligands W2 and His337 was also refined. This was carried out in two phases: first, the most likely protonation pattern was determined in the S_1-state; then, more reduced states of the Mn cluster were also explored. More details on the procedure are discussed in the Computational Methods.

In all computations carried out in the present study, the main criterion used to identify the proper oxidation and protonation states is the agreement with the PSII crystal structure.[16] The electronic energy is only used as a second rank criterion. States of the Mn cluster, which differ only in the alignments of local Mn spins, can be very close in electronic energies[22] and are therefore difficult to discriminate energetically. But, at the same time, they virtually possess the same geometry,[23] that is, the precise nature of the local spin alignment is not critical for the present study. Electronic energies of complex systems like the Mn cluster are only comparable, if one considers the same oxidation state and the same number of protons. We used such energy comparison only for the S_1-state of the Mn cluster (see Table 1). Details on the choice of the local spin alignments are described in the Computational Methods, section on Quantum Chemistry.

Stage 1: Protonation of Mn-CORE. In stage 1, all possible 18 different protonation patterns of the Mn-CORE were explored in the S_1-state (see Figure 2). The 18 protonation states were sorted into six groups, which differ by the total charge of the OEC-model. Models belonging to the same group contain the same number of atoms. Therefore, a direct energy comparison is possible. Computed relative energies and root-mean-square deviations of the Mn-CORE (rmsd$_{CORE}$) from the crystal structure are given in Table 1.

Our data suggest that the protonation patterns O5HH− O4HH and O5HH−O4HH−O1H (entries 15 and 18 in Table 1) are not stable in the S_1-state, that is, the oxygen atom O4 spontaneously loses a proton during geometry optimization. Therefore, these models were not considered for further analysis. In addition, comparison of relative energies within each charge group reduces the number of the possible OEC-models to five (bold characters in Table 1). For these five structures, further calculations in different oxidation states (S_0 to S_{-4}) were performed in stage 2. In group III, the energy difference between the OEC-models 6 and 9 is too small

(smaller than 3 kcal/mol) to exclude the latter. Therefore, model 9 was considered also in stage 2 for further calculations.

The smallest rmsd value of the 16 stable Mn-CORE structures considered in the S_1-state (Table 1) is slightly above 0.2 Å. This is larger than the average precision of the atomic coordinates in the high resolution PSII crystal structure, 0.16 Å.[16] Previous studies[23] demonstrated that atom pair distances of simple manganese model clusters optimized at DFT level deviate less than a few hundreds of angstroms from crystal structures. Similar results were also reported in our recent work where the same level of theory was employed to study di-manganese clusters.[24] It was also found that two geometrical parameters (Mn−Mn and Mn−O distances) are particularly sensitive to protonation changes. Interestingly, specific Mn−Mn and Mn−O distances vary significantly with the protonation pattern. The maximum distance changes observed in our computations are about 0.44 Å for Mn4−O4 and Mn4−O5. Variations of these two distances between computed and crystal structures are indeed the main contributors to the rmsd values of the Mn-CORE (Table 1).

Stage 2: Oxidation of Mn-CORE. Considering the intensity of synchrotron radiation in the experiments, the OEC may be reduced to states below S_1. To explore this point, an additional five oxidation states were investigated besides the S_1-state. These are schematically $S_0[Mn_4(II,III,IV,IV)]$, $S_{-1}[Mn_4(II,III,III,IV)]$, $S_{-2}[Mn_4(II,III,III,III)]$, $S_{-3}[Mn_4(II,II,III,III)]$, and $S_{-4}[Mn_4(II,II,II,III)]$. With the present quantum chemical approach, the total oxidation states of the Mn cluster are precise, while the degrees of oxidation of the individual Mn are fractional as is the case for real multicore transition metal complexes. Integer valued oxidation states of individual Mn can be enforced only by applying artificial constraints. In this sense, notations about the oxidation state of the Mn cluster like $Mn_4(II,II,II,III)$ serve only as a rough orientation. The precise fractional oxidation states of the four Mn can be inferred from local spin densities that are given in Table S10 of the Supporting Information.

Two definitions of rmsd values relative to the PSII crystal structure were considered. The $rmsd_{CORE}$ involves only the 10 atoms of the Mn-CORE. The $rmsd_{CORE+HOH}$ includes also the oxygen atoms of the crystal waters HOH358, HOH428, HOH446, HOH538, HOH539, HOH542, HOH923, HOH540, HOH541, HOH999 (W2), and HOH1000 (W1). The other ligands of the Mn cluster are not considered in rmsd values, since they are fixed in their crystal structure position. The results for the most promising OEC-models 1, 3, 6, 13, and 17 are displayed in Figure 3.

Figure 3 shows that the smallest deviations from the experimental structure were obtained for the protonation pattern of model 6 (O5H−O4H−His337+−W2−). Deviations are even smaller when the $Mn_4CaO_5^-$ cluster is reduced to the S_{-3}-state, which corresponds to the formal oxidation state $Mn_4(II,II,III,III)$. This agreement with the crystal structure of the Mn cluster confirms previous hypothesis,[8−10,17,18] and strongly suggest that the PSII crystal has suffered reductive damage due to excess synchrotron radiation. Notably, the $rmsd_{CORE}$ of model 6 is only 0.162 Å ($rmsd_{CORE+HOH}$ = 0.120 Å) in the S_{-3}-state, which is in the range of the experimental uncertainty (~0.16 Å).[16] Thus, according to our data, the protonation pattern of model 6 is the most suitable to the PSII crystal structure. Therefore, model 6 was considered for further calculations in stage 3, where the protonation of the Mn-CORE-extended (Mn_4CaO_5−W2-His337) was considered.
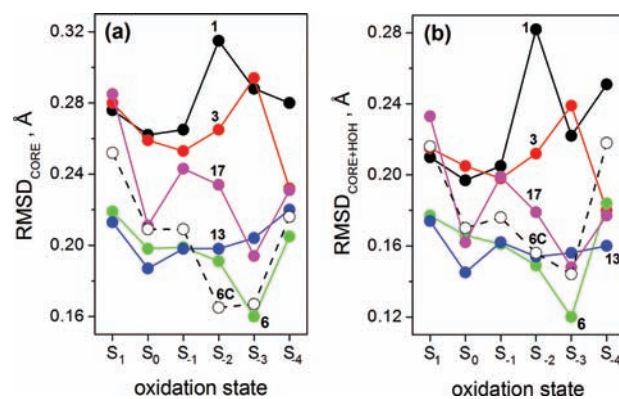

Figure 3. Dependence of $rmsd_{CORE}$ (a) and $rmsd_{CORE+HOH}$ (b) on the oxidation states of the OEC-model observed for models 1, 3, 6, 13, 17, and 6C. The OEC-models (excluding 6C) use for W2 the OH^- form and His337+. Model 6C (open circles, dashed line) considers W2 in the H_2O form. For the sake of clarity, the large rmsd values of model 9 are not included in the graphs. The numerical values of the rmsd values for models 1, 3, 6, 9, 13, and 17 are given in Table S3 of the Supporting Information.

Stage 3: Protonation of the Mn-CORE-Extended. On the basis of the protonation state of model 6 (O5H−O4H−His337+−W2−), three additional protonation patterns were explored in stage 3. By changing the protonation of W2 and that of His337, models 6A, 6B, 6C were obtained (Table 2). In line with the results of the selection procedure applied in stage 1, the analysis of the relative energies suggest model 6C has the most relevant protonation state in charge group IV, while those of models 6A and 6B are not likely (Table 2). To find the best match between model and experimental structure, the structure of model 6C was optimized in different oxidation states, from S_1 to S_{-4} (Table S3). Notably, the lowest $rmsd_{CORE}$ (0.164 Å) of model 6C was found in the S_{-2}-state (Figure 3, Table S3).

Interestingly, when the degree of reduction increases from S_1 to S_{-3}, the excess proton at His337+ in models 6 and 6C is spontaneously transferred to O3 during geometry optimization. While this transfer occurs between states S_{-2} and S_{-3} for model 6, it happens already between the oxidation states S_{-1} and S_{-2} for model 6C. Remarkably, this finding agrees well with our recent results obtained via a DFT-based empirical model that qualitatively predicts protonation patterns of small manganese clusters from their structure.[24]

As a result of the three-stage procedure, two possible protonation patterns (6 and 6C, see Figure 4) were found that have comparable $rmsd_{CORE}$ values in the reduced S-states (Figure 3, Table S3). Both OEC-models show structural variations with the oxidation states. The smallest deviations to the crystal structure are observed for model 6 and 6C in the S_{-3}- and S_{-2}-states, respectively. A detailed analysis of specific structural parameters of these two Mn cluster models shows that model 6C deviates from the crystal structure more significantly than model 6. In particular, the maximum deviations are 0.24 Å (Mn2−O2 bond) and 0.17 Å (Mn3−O2 bond) for model 6C and for model 6, respectively (Figure 5 and Table S4). Indeed, model 6 shows the smallest $rmsd_{CORE}$ (0.16 Å) and $rmsd_{CORE+HOH}$ (0.12 Å), to be compared to 0.164 and 0.156 Å, respectively, of model 6C. Additionally, the bond lengths of Mn4 to the ligand waters W1 and W2 are reproduced by model 6 within the experimental uncertainty, while for model 6C, the discrepancies are larger (Table S5). Thus, the data obtained through the three-stage procedure

Table 2. Protonation States of the S₁-State of the OEC-Models 6A, 6B, and 6C from Stage 3 (Protonation of Mn-CORE-Extended) Are Compared with the Models 3, 6, and 13 from Stage 1 (Protonation of Mn-CORE)[a]

charge group	no.	protonation state	rmsd$_{CORE}$ [Å]	relative energy [kcal/mol]
II	3.	**O5−O4H−His337⁺−W2⁻**	**0.280**	**0.00**
	6A.	O5H−O4H−His337°−W2⁻	0.221	16.19
III	6.	**O5H−O4H−His337⁺−W2⁻**	**0.219**	**0.00**
	6B.	O5H−O4H−His337°−W2°	0.227	25.31
IV	13.	O5H−O4H−O1H−His337⁺−W2⁻	0.212	13.85
	6C.	**O5H−O4H−His337⁺−W2°**	**0.252**	**0.00**

[a]The rmsd values are given relative to the PSII crystal structure.[16] Relative energies are comparable only within the same charge group where the protonation states involve the same number of protons. The models with lowest energy in each group are rendered in bold.
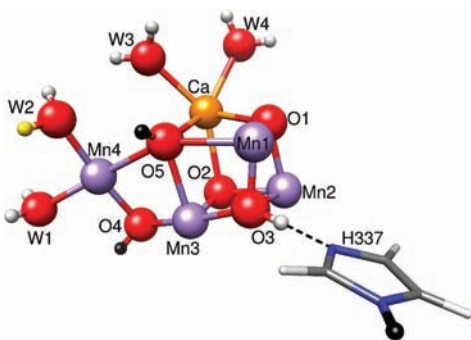

Figure 4. Protonation patterns of the two OEC-models (6 and 6C) of lowest energy and small rmsd values. Hydrogen atoms that were subject to variations in considered the protonation patterns are colored black. Model 6C differs from model 6 in possessing one additional hydrogen atom at the water W2, which is highlighted in yellow. Model 6 exhibits in the S₋₃-state the smallest deviation to the crystal structure, while model 6C shows nearly the same amount of deviation in the S₋₂- and S₋₃-states. Hydrogen bonding partners are connected by dash lines.
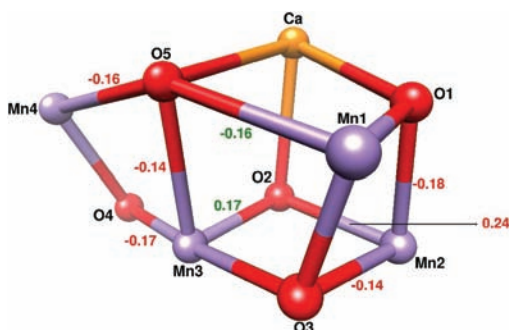

Figure 5. The deviations of the computed bond lengths from the values in the high-resolution PSII crystal structure are given for the OEC-model 6 (green) in the S₋₃-state and for the OEC-model 6C (red) in the S₋₂-state. For the sake of clarity, only deviations larger in absolute value than 0.13 Å are shown. A complete list of these bond lengths deviations is given in Table S4.

strongly suggest that the most likely protonation pattern of the OEC in the high-resolution PSII crystal structure[16] is that of model 6. Interestingly, calculation of rmsd$_{CORE}$ relative to monomer B of the PSII crystal structure confirms the small deviation (0.16 Å) for model 6 and the larger deviation for model 6C (0.195 Å) (Table S6) supporting our conclusion on the proper oxidation and protonation states in the crystal structure.

Protonation Pattern and Total Charge of the OEC-Model in the S₁-State. The most likely protonation pattern

(model 6: O5H−O4H−His337⁺−W2⁻) of the OEC-model in the S₋₃-state comprising the Mn-cluster and all its ligands (see Figure 1) has an overall charge of −1. In the more oxidized dark adapted S₁-state, this protonation pattern corresponds to a total charge of +3 for the OEC-model. However, a larger portion of this charge is localized at two positively charged ligands (Arg357 and His337), while a residual charge of +1 is delocalized over the other components of the Mn cluster. Transition metals of this size are able to host such an excess positive charge. For the function of the Mn cluster in PSII, it may even be useful that the resting S₁-state is loaded with moderate positive charge. Nevertheless, we also explore alternative protonation pattern, where the Mn cluster carries less positive charge in the S₁-state. Thus, we considered that the OEC may carry in the S₁-state one or two protons less than in the S₋₃-state removing one or both of the protons at O4 and O5. Thus, we implicitly assume that the degree of protonation of the OEC may have increased during the exposure of only a few seconds to synchrotron radiation even at liquid nitrogen temperatures.

At such low temperatures, equilibrated low energy protons may still be mobile within H-bonds but may hardly move over larger distances. The only proton, which is readily available under these conditions, is the excess proton at His337. This proton is present in the OEC-models 6C and 6. During the geometry optimization of these models, this low energy proton indeed moves spontaneously from His337⁺ to O3 when the oxidation state of the OEC is S₋₂/S₋₃ or lower. Conversely, energized excess protons may move along proton-transfer pathways formed by H-bond networks of titratable groups and water molecules. Several such proton-transfer pathways originate from the Mn cluster.[5,7,25−28] If such energized, excess protons are available, they could compensate for the accumulation of excess electrons localized in the Mn-CORE of the highly reduced S₋₃-state. Thus, one may consider the degree of protonation and its pattern found for the S₋₃-state as an upper limit of the protonation pattern in the S₁-state. We would like to remark that previous studies based on the high resolution PSII structure generally considered no protons on μ−oxo oxygens in the S₁-state.[11−15,19,20] The corresponding total charge of the OEC-model (Mn cluster with the positively charged Arg357 and its other ligands as displayed in Figure 1) in the S₁-state is than +1.

Role of Radiation Damage. It is generally agreed that synchrotron radiation can generate high energy electrons in a protein crystal, which in turn can create an avalanche of energized secondary electrons. These excess electrons can travel in a very short time over large distances through the protein crystal even at low temperatures. While doing so, they may find a suitable electron hole and recombine, and/or attach

Table 3. Protonation States of the S_1-State of the OEC-Models 1B, 1C, 2A, 2B, 2C, 3A, 3B, and 3C from the Mn-CORE-Extended (Mn_4CaO_5–H337–W2) Are Compared with the Protonation States of the Models 1, 3, and 6 Obtained from Stage 1[a]

charge group	no.	protonation state	rmsd$_{CORE}$ [Å]	relative energy [kcal/mol]	OEC charge[a]
I	**1.**	**O5–O4–H337$^+$–W2$^-$**	**0.276**	**0.40**	+1
	2A.	O5H–O4–H337°–W2$^-$	0.268	16.52	
	3A.	O5–O4H–H337°–W2$^-$	0.280	7.87	
	1B.	**O5–O4–H337°–W2°**	**0.284**	**0.00**	
II	3.	O5–O4H–H337$^+$–W2$^-$	0.280	9.12	+2
	1C.	**O5–O4–H337$^+$–W2°**	**0.279**	**0.00**	
	2B.	O5H–O4–H337°–W2°	0.246	20.13	
	3B.	O5–O4H–H337°–W2°	0.285	28.59	
III	6.	O5H–O4H–H337$^+$–W2$^-$	0.219	13.30	+3
	2C.	**O5H–O4–H337$^+$–W2°**	**0.236**	**0.00**	
	3C.	O5–O4H–H337$^+$–W2°	0.285	10.56	

[a]The rmsd values are given relative to the PSII crystal structure. The energies are comparable only within the same charge group where the protonation states involve the same number of protons. The models with lowest energy in each group are highlighted in bold characters. The corresponding absolute energies are given in Table S7 of Supporting Information. [a]Total charge of the OEC-model as depicted in Figure 1.

to an electron trap, as, for instance, the redox-active Mn cluster of PSII. It is thus not surprising that, even for short exposures to intensive synchrotron radiation at temperatures of liquid nitrogen, the Mn cluster of PSII may become highly reduced.

Having established that reduction via radiation damage may occur, the question is: are there also energized protons available in PSII under these conditions? In recent studies on protein crystal structures, the formation of H_2 gas was observed during the exposure of the crystal to intense synchrotron radiation.[29] Simultaneously, this caused a loss in high-resolution structure information. Interestingly, organic compounds rather than water molecules were identified as sources of the hydrogen atoms. Precursors of the emerging H_2 molecules are likely hydrogen atoms and protons. These protons are in an energized state and if created close enough to the Mn cluster, they may attach to it quickly also at liquid nitrogen temperatures. Hence, one or both of the μ−oxo oxygens O4 and O5 may carry no proton in the S_1-state preceding the X-ray radiation.

Model 6 is the structural model of the Mn cluster, which in the S_{-3}-state agrees best with the high-resolution crystal structure. However, based on the above remarks, we also explored the possibility of Mn cluster models that bear fewer protons in the S_1-state than does model 6 (Table 3). Interestingly, models 1C and 2C (where W2 is the neutral H_2O) are energetically more stable in the S_1−state than the alternative models of the same charge groups (II and III) with OEC-charge +2 and +3, respectively. In charge group I (OEC-charge +1) model 1B is only slightly more stable than model 1. However, lowering the oxidation state for those three OEC-models (1B, 1C, 2C) results in rmsd values relative to the crystal structure (Table S8) much larger than for the model 6. Notably, model 2C, when in the S_1-state, is about 13 kcal/mol more stable than model 6, whose protonation pattern likely pertains to the S_{-3}-state of the PSII crystal structure. Hence, we conclude that the protonation pattern of model 2C is likely a candidate for the S_1-state of the Mn cluster. However, OEC-models with the lower total charge (+2 for model 1C and +1 for model 1 and 1B, see Table 3) may also be possible. As the level of reduction increases, model 6 becomes more likely. Unfortunately, the models 1B (1), 1C, 2C (Table 3) can energetically not be compared, since they differ in the number of protons. Although, it is not likely that the protonation state of the Mn cluster in the high-resolution crystal structure differs

much from the S_1-state (as we assumed in our approach), we cannot exclude that protonation patterns with less protons may be relevant in the S_1-state.

Combined OEC-Model Structure. The set of optimized OEC-model structures discussed in the previous sections was also employed to estimate the simultaneous contribution of different S-states to the structure of the OEC in the PSII crystal. To do so, a linear combination of OEC structures based on model 6 at different oxidation states (S_1−S_{-4} with the protonation pattern of model 6) was calculated according to eq 1, as described in the Computational Methods. This analysis reveals that the OEC structure is a mixture of S_{-4} (2%), S_{-3} (56%), S_{-2} (16%), S_{-1} (12%), and S_0 (14%) (Figure S3). Therefore, the S_{-3}-state is by far the main contribution to the electron density of the Mn cluster in the PSII crystal structure. Importantly, the rmsd values of the combined OEC structure based on quantum chemical computations is significantly smaller (rmsd$_{CORE}$ = 0.135 Å and rmsd$_{CORE+HOH}$ = 0.105 Å) relative to the crystal structure compared to the OEC structure of the pure S_{-3}-state. These results are consistent with the assumption that the S_1-state is present in the PSII crystal before the exposure to synchrotron radiation and that during the X-ray measurements, the Mn cluster is converted to highly reduced forms.

■ CONCLUSIONS

On the basis of the newest high-resolution (1.9 Å) crystal structure of PSII,[16] multiple protonation patterns combined with different oxidation states of the oxygen-evolving complex were investigated. The oxidation state S_1 was initially studied, since it is the oxidation state in which the PSII crystal was prepared. By employing a three-stage procedure, the most reasonable 72 protonation patterns and six different oxidation states (S_1 to S_{-4}) were explored. The best agreement with the experimental structure was found for the OEC-model 6 in the S_{-3}-state. This structure shows deviations from the PSII crystal structure, which are within the experimental uncertainty of the atomic coordinates of about 0.16 Å. A detailed analysis of the bond lengths (Figure 5) confirms that the most likely protonation pattern is that of model 6 as depicted in Figure 4. Therefore, for this protonation pattern, all possible oxidation states were explored. In line with previous studies,[8−10,17,18] our data strongly suggest that the PSII crystal has suffered radiation damage and the Mn cluster is most likely in the S_{-3}-state.

A linear combination of the optimized structures based on the OEC-model 6 in different oxidation states strongly suggests that the S$_{-3}$-state contributes dominantly to the electron density of the crystal structure. The hypothesis that the OEC in the PSII crystal structure may be a mixture of lower oxidation states was recently put forward.[1,17] Our work confirms and quantifies this finding, that is, the main contribution (nearly 60%) is from the S$_{-3}$-state.

While being reduced, the Mn cluster may also increase its degree of protonation, as energized, excess protons are generated by synchrotron radiation in the protein simultaneously with free electrons. According to our results, the protonation pattern of model 6 is the most suitable for the S$_{-3}$-state, where the OEC-charge is −1. In the S$_1$-state, however, the same protonation pattern would result in a Mn cluster with a charge of +3 for the OEC-model (Figure 1), which may be too positive. In model 6, both μ−oxo oxygens connected with the dangling manganese Mn4, O4 and O5, carry a proton. In this sense, model 6 can be considered as a limit state with maximum degree of protonation. In the S$_1$-state the Mn unit, Mn$_4$CaO$_5$−H337−W2, may carry less protons, but not necessarily at other positions than in model 6.

To avoid a large positive OEC-charge of +3 in the S$_1$-state as for instance in model 6, the two μ−oxo oxygens O4 and O5 may carry no protons. This condition is fulfilled in the models 1, 1B and 1C, where the OEC-model carries total charges of +1 and +2, respectively (Table 3). With a total charge of +2 in the S$_1$-state the most appropriate protonation pattern of the OEC-model is 1C (Table 3). In this OEC-model, there are no protons on O5 and O4, W2 is a charge neutral water and His337 protonated. However, to confirm the protonation state of the Mn cluster in the S$_1$-state, computations of the pK_a values of the different possible protonation pattern of the Mn cluster will be necessary. Such computations would require high-level quantum chemistry combined with an electrostatic approach that can account for the long-range charge−charge interactions in the protein environment. However, it is unclear whether such computations can be performed for the Mn cluster at the necessary accuracy of 1 to 2 pH units with the methods available up to now.

The oxidation state S$_{-3}$ predominant in the PSII crystal structure is functionally not relevant but may exhibit structural details and protonation pattern that are closely related to the dark adapted functional S$_1$-state. A precise and structurally faithful understanding of the protonation pattern in the S$_{-3}$-state is an important anchor point to construct the oxidation and protonation states involved in the Kok reaction cycle of the OEC. Hence, analyzing the nature of the state of the Mn cluster in the PSII crystal structure provides the crucial information that is necessary for a first step toward understanding of OEC function.

■ COMPUTATIONAL METHODS

Quantum Chemistry. All DFT calculations were carried out with Jaguar 7.7.[30] Geometry optimizations were performed using the B3LYP[31−34] functional combined with LACVP,[35] an effective core potential for transition metal atoms and 6-31G** basis set for all other atoms. This level of theory has been shown to reproduce accurately experimental structures of Mn clusters similar to those studied here.[11,24]

The correct local spin alignment of the individual Mn metal centers of the OEC is not obvious. Using a broken symmetry approach, it was found that electronic energies of the Mn cluster in the same oxidation state but with different local spin alignments can be very close.[22] We

used the total spin S = 0, as determined for the S$_1$-state from EPR-measurements,[36] which corresponds to antiferromagnetic coupling. Details on the local spin densities of the four Mn obtained by Jaguar 7.7[30] are given in the Supporting Information. Since the optimized geometries of the Mn cluster are virtually independent from the spin alignment,[23] this procedure is not critical for the present application.

OEC-Models. The Mn$_4$CaO$_5$ cluster and the protein ligands Asp170, Glu189, His332, Glu333, Asp342, Ala344, Glu354, as well as water molecules HOH540, HOH541, HOH999, HOH1000 were included in the DFT calculation together with further 13 nearby residues (Tyr161, His190, His337, Arg357, HOH358, HOH428, HOH446, HOH538, HOH539, HOH542, HOH543, HOH548, HOH923)[16] involved in hydrogen bonds with Mn$_4$CaO$_5$ or its ligands. We henceforth define this molecular setup as OEC-model (see Figure 1). The OEC-models used in this study were constructed based on the PSII crystal structure of monomer A.[16] In monomer B, a number of cofactors are missing, which are however not critical for OEC function.[16] The rmsd values of OEC-model atoms and especially of Mn$_4$CaO$_5$ atoms between monomers A and B are less than 0.12 Å. The rmsd value for water molecules included in OEC-model between two monomers is, with 0.165 Å, slightly higher, but still within the experimental uncertainty. The total number of atoms of the considered OEC-models ranges between 141 and 146, depending on the protonation states. Note that we make of use of the following notation: W1, W2, W3, and W4 for the water ligands HOH1000, HOH999, HOH541, and HOH540.

Geometry Optimization. To geometrically constrain loose ends of residues on the boundary of the considered OEC-model, the atoms of Tyr161, His190, His337, Arg357, Asp170, Glu189, His332, Glu333, Asp342, Ala344, Glu354 and the water oxygens of HOH543 and HOH548 were fixed in all quantum chemical computations. Similarly, spatially fixed dummy atoms [Asp61(C$_\beta$, C$_\gamma$, O$_{\delta 1}$, O$_{\delta 2}$), Ser169(C$_\alpha$, C$_\beta$, O$_\gamma$), Asn181(C$_\beta$, C$_\gamma$, O$_{\delta 1}$, O$_{\delta 2}$), HOH398(O) and HOH778(O)] were used to constrain artificially defined torsion angles of the OEC-model (see Figure S1). To achieve a trade-off between number of atoms and computational efficiency, amino acid residues were truncated as follows: Asp and Glu were represented by acetates, His by imidazoles; Tyr by phenols and Arg by guanidinium ion. Hydrogen atoms were added by taking into account the standard protonation state of residues at physiological pH. As described above, alternative protonation patterns of the OEC-model and its ligands W2 and His337 were considered.

To optimize the geometry of the OEC-model, a three-step procedure was employed: (1) only hydrogens were optimized; (2) geometry optimization was carried out with fixed experimental torsion angles; (3) Mn$_4$CaO$_5$ geometry was optimized by fixing all non-hydrogen atoms not belonging to it.

Energy Calculation. The protein environment, which is not included in the OEC-model explicitly, was represented as a dielectric continuum with dielectric constant ε = 15. The strategy for the correct choice of the dielectric constant for a protein environment is discussed in the literature.[37,38] These protein environment contributions to the OEC-model energy were evaluated as solvation energy, computed by solving the Poisson equation with the program module "Solvate" from MEAD.[39,40] The atomic partial charges used in "Solvate" were calculated as described in previously[41] using the RESP procedure.[42,43] Solvation parameters like solvent probe radius (1.4 Å) and atomic radii of the OEC-model were also adopted from the literature.[41] These are (in Å) for H, C, N, O, and Mn, 1.0, 1.65, 1.60, 1.60, and 1.48, respectively.

Exploring Protonation States. In the first stage (protonation of Mn-CORE), all possible protonation states of O1, O4 and O5 in Mn$_4$CaO$_5$ were explored. W2 kept fixed as OH$^-$ and His337 was kept protonated. By comparing the energies (see Table 1), the optimal protonation patterns of the Mn$_4$CaO$_5$ were determined at this stage. The protonation patterns selected in the first stage were further considered for calculations in the second stage (oxidation of Mn-CORE), where the additional five oxidation states S$_0$ to S$_{-4}$ were explored. Deviations from the crystal structure, measured in rmsd's, were employed as selection criterion. The protonation patterns that

showed rmsd's from the crystal structure ranging within the experimental uncertainty, ~0.16 Å, were then used for calculations in the third stage (protonation of Mn-CORE-extended). In this stage, the protonation pattern chosen from the stage 2 (oxidation of the Mn-CORE) was kept fixed while changing the protonation of the Mn_4CaO_5 ligands W2 and His337.

Linear Combination of Optimized OEC-Model Structures in Different Oxidation States. Coordinates of OEC-model structures, S_{comb}, were computed from linear combinations of OEC-models at six different oxidation states (S_1 to S_{-4}) minimizing the rmsd relative to the crystal structure according to

$$a_1S_1 + a_2S_0 + a_3S_{-1} + a_4S_{-2} + a_5S_{-3} + a_6S_{-4} = S_{comb} \qquad (1)$$

The coefficients a_i, constrained to $a_i > 0$, $\sum a_i = 1$, provide the contributions for the oxidation states S_1 to S_{-4}. The S_{comb} structure with the lowest $rmsd_{CORE+HOH}$ is determined exploring all a_i values in the interval $[0, 1]$ using increments of 0.01.

■ ASSOCIATED CONTENT

ⓢ Supporting Information

Detailed information on OEC-model, energies, rmsd, interatomic distances, coordinates charges, and local spin densities. This material is available free of charge via the Internet at http://pubs.acs.org.

■ AUTHOR INFORMATION

Corresponding Author
knapp@chemie.fu-berlin.de

Notes

The authors declare no competing financial interest.

■ ACKNOWLEDGMENTS

■ REFERENCES

(1) A preliminary account of this work in particular the identification of the proper reduction state of the Mn-cluster in 1.9 Å crystal structure and its corresponding protonation state was reported at the conference "Photosynthesis Research for Sustainability", Baku, July 24−30, 2011.
(2) Leslie, M. *Science* **2009**, *323*, 1286−1287.
(3) Zouni, A.; Witt, H.-T.; Kern, J.; Fromme, P.; Krauß, N.; Saenger, W.; Orth, P. *Nature* **2001**, *409*, 739−743.
(4) Kamiya, N.; Shen, J.-R. *Proc. Natl. Acad. Sci. U.S.A.* **2003**, *100*, 98−103.
(5) Ferreira, K. N.; Iverson, T. M.; Maghlaoui, K.; Barber, J.; Iwata, S. *Science* **2004**, *303*, 1831−1838.
(6) Loll, B.; Kern, J.; Saenger, W.; Zouni, A.; Biesiadka, J. *Nature* **2005**, *438*, 1040−1044.
(7) Guskov, A.; Kern, J.; Gabdulkhakov, A.; Broser, M.; Zouni, A.; Saenger, W. *Nat. Struct. Mol. Biol.* **2009**, *16*, 334−342.
(8) Dau, H.; Liebisch, P.; Haumann, M. *Phys. Chem. Chem. Phys.* **2004**, *6*, 4781−4792.
(9) Grabolle, M.; Haumann, M.; Müller, C.; Liebisch, P.; Dau, H. *J. Biol. Chem.* **2006**, *281*, 4580−4588.
(10) Yano, J.; Kern, J.; Irrgang, K.-D.; Latimer, M. J.; Bergmann, U.; Glatzel, P.; Pushkar, Y.; Biesiadka, J.; Loll, B.; Sauer, K.; Messinger, J.; Zouni, A.; Yachandra, V. K. *Proc. Natl. Acad. Sci. U.S.A.* **2005**, *102*, 12047−12052.
(11) Sproviero, E. M.; Gascon, J. A.; McEvoy, J. P.; Brudvig, G. W.; Batista, V. S. *J. Am. Chem. Soc.* **2008**, *130*, 3428−3442.
(12) Siegbahn, P. E. M. *Chem.—Eur. J.* **2008**, *14*, 8290−8302.
(13) Siegbahn, P. E. M. *Acc. Chem. Res.* **2009**, *42*, 1871−1880.
(14) Siegbahn, P. E. M. *Dalton Trans.* **2009**, 10063−10068.
(15) Siegbahn, P. E. M. *J. Photochem. Photobiol., B* **2011**, *104*, 94−99.
(16) Umena, Y.; Kawakami, K.; Shen, J.-R.; Kamiya, N. *Nature* **2011**, *473*, 55−61.
(17) Luber, S.; Rivalta, I.; Umena, Y.; Kawakami, K.; Shen, J.-R.; Kamiya, N.; Brudvig, G. W.; Batista, V. S. *Biochemistry* **2011**, *50*, 6308−6311.
(18) Grundmeier, A.; Dau, H. *Biochim. Biophys. Acta* **2012**, *1817*, 88−105.
(19) Ames, W.; Pantazis, D. A.; Krewald, V.; Cox, N.; Messinger, J.; Lubitz, W.; Neese, F. *J. Am. Chem. Soc.* **2011**, *133*, 19743−19757.
(20) Siegbahn, P. E. M. *Chem. Phys. Chem.* **2011**, *12*, 3274−3280.
(21) Yano, J.; Kern, J.; Sauer, K.; Latimer, M. J.; Pushkar, Y.; Biesiadka, J.; Loll, B.; Saenger, W.; Messinger, J.; Zouni, A.; Yachandra, V. K. *Science* **2006**, *314*, 821−825.
(22) Kanda, K.; Yamanaka, S.; Saito, T.; Umena, Y.; Kawakami, K.; Shen, J.-R.; Kamiya, N.; Okumura, M.; Nakamura, H.; Yamaguchi, K. *Chem. Phys. Lett.* **2011**, *506*, 98−103.
(23) Sproviero, E. M.; Gascon, J. A.; McEvoy, J. P.; Brudvig, G. W.; Batista, V. S. *J. Inorg. Chem.* **2006**, *100*, 786−800.
(24) Robertazzi, A.; Galstyan, A.; Knapp, E. W. *Cryst. Eng. Comm.* **2011**, *13*, 6369−6372.
(25) Ishikita, H.; Saenger, W.; Loll, B.; Biesiadka, J.; Knapp, E.-W. *Biochemistry* **2006**, *45*, 2063−2071.
(26) Murray, J. W.; Barber, J. *J. Struct. Biol.* **2007**, *159*, 228−237.
(27) Ho, F. M.; Styring, S. *Biochim. Biophys. Acta* **2008**, *1777*, 140−153.
(28) Ho, F. M. *Photosynth. Res.* **2008**, *98*, 503−522.
(29) Meents, A.; Gutmann, S.; Wagner, A.; Schulze-Briese, C. *Proc. Natl. Acad. Sci. U.S.A.* **2010**, *107*, 1094−1099.
(30) *Jaguar*; 7.7 ed.; Schrödinger, L.L.C.: New York, 2010.
(31) Becke, A. D. *Phys. Rev. A* **1988**, *38*, 3098−3100.
(32) Lee, C.; Yang, W.; Paar, R. G. *Phys. Rev. B* **1988**, *37*, 785−789.
(33) Slater, J. C. *Quantum Theory of Molecules and Solids*; McGraw-Hill: New York, 1974; Vol. 4.
(34) Vosko, S. H.; Wilk, L.; Nusair, M. *Can. J. Phys.* **1980**, *58*, 1200−1211.
(35) Hay, P. J.; Wadt, W. R. *J. Chem. Phys.* **1985**, *82*, 299−310.
(36) Koulougliotis, D.; Hirsh, D. J.; Brudvig, G. W. *J. Am. Chem. Soc.* **1992**, *114*, 8322−8323.
(37) Schutz, C. N.; Warshel, A. *Proteins* **2001**, *44*, 400−417.
(38) Galstyan, A. S.; Zarić, S. D.; Knapp, E. W. *J. Biol. Inorg. Chem.* **2005**, *10*, 343−354.
(39) Bashford, D.; Gerwert, K. *J. Mol. Biol.* **1992**, *224*, 473−486.
(40) Bashford, D. In *ISCOPE97*; Springer: Berlin, 1997; pp 233−240.
(41) Galstyan, A. S.; Knapp, E. W. *J. Comput. Chem.* **2009**, *30*, 203−211.
(42) Bayly, C.; Cieplak, P.; Cornell, W.; Kollman, P. *J. Phys. Chem.* **1993**, *97*, 10269−10280.
(43) Cornell, W.; Cieplak, P.; Bayly, C.; Kollman, P. *J. Am. Chem. Soc.* **1993**, *115*, 9620−9631.